Journal of Pharmacokinetics and Pharmacodynamics (2019) 46:339–359
https://doi.org/10.1007/s10928-019-09640-9

ORIGINAL PAPER

Computer-assembled cross-species/cross-modalities two-pore physiologically based pharmacokinetic model for biologics in mice and rats

Armin Sepp[1] · Guy Meno-Tetang[5,6] · Andrew Weber[2] · Andrew Sanderson[3] · Oliver Schon[3,4] · Alienor Berges[5,7]

Received: 19 December 2018 / Accepted: 5 May 2019 / Published online: 11 May 2019

Abstract

Two-pore physiologically-based pharmacokinetic (PBPK) models can be expected to describe the tissue distribution and elimination kinetics of soluble proteins, endogenous or dosed, as function of their size. In this work, we amalgamated our previous two-pore PBPK model for an inert domain antibody (dAb) in mice with the cross-species platform PBPK model for monoclonal antibodies described in literature into a unified two-pore platform that describes protein modalities of different sizes and includes neonatal Fc receptor (FcRn) mediated recycling. This unified PBPK model was parametrized for organ-specific lymph flow rates and the endosomal recycling rate constant using an extended tissue distribution time-course dataset that included an inert dAb, albumin and IgG in rats and mice. The model was evaluated by comparing the ab initio predictions for the tissue distribution and elimination properties of albumin-binding dAbs (AlbudAbs™) in mice and rats with the experimental observations. Due to the large number of molecular species and reactions involved in large-scale PBPK models, we have also developed and deployed a Matlab™ script for automating the assembly of SimBiology™-based two-pore biologics PBPK models which drastically cuts the time and effort required for model building.

Keywords Domain antibody · AlbudAb™ · Albumin · Antibody · Physiologically based pharmacokinetics

Electronic supplementary material The online version of this article (https://doi.org/10.1007/s10928-019-09640-9) contains supplementary material, which is available to authorized users.

✉ Armin Sepp
armin.z.sepp@gsk.com

1 Systems Modeling and Translational Biology, 1F307 Glaxo Medicines Research Centre, GlaxoSmithKline, Stevenage SG1 2NY, UK

2 Systems Modeling and Translational Biology, GlaxoSmithKline, King of Prussia, PA 19406, USA

3 PCS R&D, GlaxoSmithKline, Stevenage SG1 2NY, UK

4 Present Address: AgenusBio, 315 Cambridge Science Park, Milton Road, Cambridge CB4 0WG, UK

5 Clinical Pharmacology, Modelling and Simulation, GlaxoSmithKline, Stockley Park, Uxbridge UB11 1BT, UK

6 Present Address: Modeling & Simulation, Immunology/Inflammation, UCB Pharmaceuticals, 208 Bath Road, Slough SL1 3WE, UK

7 Present Address: Quantitative Clinical Pharmacology, Early Clinical Development, IMED Biotech Unit, AstraZeneca, Cambridge, UK

Introduction

In addition to monoclonal antibodies (mAbs), an increasing number of newly engineered immunotherapeutic modalities are making their way towards the clinic [1, 2], including fully human heavy and light chain variable domain antibodies (dAbs) [3–5], nanobodies® [6] and VNAR domains [7]. The albumin-binding dAbs (AlbudAbs™) [8] and other similar modalities benefit from the extended albumin-like plasma half-life and can be fused or conjugated to a therapeutics payload of interest. For the optimal use of those and other emerging therapeutic protein modalities, it is desirable to evaluate their whole-body kinetics and requirements for target engagement in organs of interest in the early phase of drug development.

Physiologically based pharmacokinetics (PBPK) is a quantitative systems approach that allows investigating drug disposition characteristics between tissues and across different species. These models make use of species-specific organ and vascular compartment volumes and their respective blood flow rates. PBPK models describing

biologics also divide the extravascular region into intracellular and interstitial compartments and include the lymphatic circulation as well. Proteins do not diffuse across plasma membranes and in the two-pore based PBPK model [9–13], their extravasation from plasma to interstitial space is described as a filtration-diffusion transport process via paracellular pores which is driven by the hydrostatic pressure and concentration gradients respectively. In addition, an endosomal compartment accounting for the FcRn-mediated recycling and transcytosis is included as per Garg and Balthasar [14, 15].

In our previous paper [12], we described a PBPK model for an inert dAb construct in mice which was based on the two-pore hypothesis of extravasation by Rippe and Haraldsson [16]. In particular, we demonstrated, theoretically and experimentally, that the organ-specific isogravimetric flow rates ($J_{org,ISO}$) and permeability-surface area products (PS_{org}) can be expressed as linear functions of the lymph flow rate (J_{org}) [12], thereby eliminating a major source of uncertainty and overparameterization. In addition, we introduced a size-dependent glomerular filtration of plasma proteins in the kidney. However, the endosomal recycling aspect of the model was not considered because of the absence of neonatal Fc receptor (FcRn) binding activity of the dAb used. We showed that the relative contribution of filtration and diffusion to the process of extravasation depends on the size of the protein. In the case of smaller proteins, like dAbs, diffusion dominates, while in the case of larger ones, filtration is sufficient to describe their tissue disposition, as in the cross-species platform PBPK model for mAbs by Shah and Betts [17].

In this paper we amalgamate our previously developed two-pore model [12] with the cross-species platform for antibodies by Shah and Betts [17] to provide a framework that can describe the distribution and extravasation of soluble proteins, whilst considering the impact of FcRn-mediated recycling and transcytosis, when applicable.

The unified PBPK model was parameterized using the tissue distribution time course data obtained in mice and rats for inert dAbs, albumin and mAbs, considering their respective sizes and FcRn-binding properties. We then qualified the model using tissue distribution and plasma half-life data of various AlbudAbs™ with different affinities to albumin to extend their plasma half-life and tissue distribution.

PBPK models for biologics can include many interacting endogenous and exogenous proteins at the same time. As a result, the model building process becomes increasingly labour-intensive due to the large number of molecular species, binding reactions and extravasation processes involved that need to be defined for each model compartment. In an effort to accelerate the model building process, we developed a Matlab™ script for computer-assisted assembly of SimBiology™-compliant two-pore biologics PBPK models that can be used for optimisation, simulation, and cross-species dose prediction purposes.

Materials and methods

Modalities

The following modalities were used for the development and validation of the unified platform PBPK model and are listed in Table 1.

1. DMS5558 dAb2, which has been described previously [12], is an inert fusion protein of two dAbs with no known binding activity, where the C-terminus of human germline VH dAb is linked to the N-terminus of human germline Vk dAb via Alanine-Serine-Threonine (AST) tripeptide linker.
2. MSA is mouse serum albumin (Sigma, Dorset, UK) purified by size exclusion chromatography on HiLoad 16/600 Superdex 75 pg column (GE Healthcare, Hatfield, UK) to isolate the monomeric fraction.
3. RSA is rat serum albumin purified from rat plasma (Innovative Research Inc., Navi, USA) by affinity chromatography on HiScreen Capto Blue 5 ml column (Sigma, Dorset, UK) followed by size exclusion chromatography on HiLoad 16/600 Superdex 75 pg.
4. Mouse IgG1 data (mIgG1) is from the papers by Garg and Balthasar [14] and Baxter et al. [9].
5. GSK679586 is a human IgG1 (hIgG1) with no known binding activity for rat antigens.
6. DMS5538 dAb2 is identical to DMS5588 dAb2 except that the N-terminal germline VH dAb is fused via AST to the albumin-binding human Vk dAb (AlbudAbTM DOM7h-11-12).
7. A selection of AlbudAbsTM with affinities for albumin ranging from 3 nM to 1.3 μM, as measured by surface plasmon resonance on Biacore 3000 with albumin immobilized on CM5 chips by amine coupling.

DMS5558, DMS5538, GSK679586 and all AlbudAbs™ are from GlaxoSmithKline Plc. (GSK, Stevenage, UK).

Experimental data

All proteins used in tissue distribution studies were radiolabelled by Quotient Bioresearch (Rushden) Ltd. (Rushden, UK) using *N*-succinimidyl[2,3-^{3}H] propionate (^{3}H-NSP) from Perkin-Elmer (Seer Green, UK). DMS5558 and DMS5538 were dosed intravenously (IV) at 10 mg/kg both in mice and rats. Albumin was administered IV to mice and rats at 2.5 mg/kg. GSK679586 was dosed IV at 2.5 mg/kg in rats only. Mouse tissue distribution studies were

Table 1 Modalities data used to optimise and validate the PBPK model

Modality	Structure	Name	Species	Data source
Training set				
Non-specific dAb2		DMS5558	Normal mice and rats	GSK
Mouse Albumin		MSA	Normal mice	GSK
Rat Albumin		RSA	Normal rat	GSK
Mouse IgG1	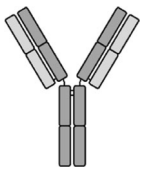	mIgG1 (7E3)	Normal mice	Literature [14]
Mouse IgG1	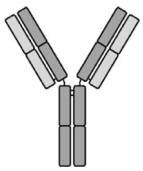	mIgG1 (MOPC21)	Nude mice	Literature [9]
Human IgG1	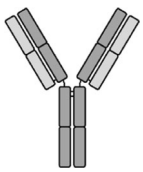	hIgG1 (GSK679586)	Normal Rat	GSK
Validation set				
Murine IgG1	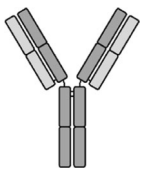	mIgG1 (7E3)	FcRn KO mice	Literature [14]
dAb-AlbudAb™		DMS5538	Normal mice	GSK
AlbudAbs™	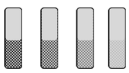		Normal mice	GSK

performed by quantitative whole-body autoradiography (QWBA), as described previously [12]. Rat tissue distribution studies were carried out by quantitative radiochemical analysis (QRA) directly (for plasma only) or indirectly, by prior oxidation of tissue samples followed by liquid scintillation counting of the released tritium. In addition, rat tissue sections were analysed qualitatively by autoradiography. Animal experiments were performed by Quotient Bioresearch (Rushden) Ltd. using female CrC:CD1, albino mice weighing 26–33 g and albino rats (Crl:CD1) weighing 176–232 g. All animal studies were ethically reviewed and carried out in accordance with the Animals (Scientific Procedures) Act 1986 and the GSK Policy on the Care, Welfare and Treatment of Animals.

All IgG data in C57BL/6 mice and FcRn-knock-out (KO) mice were extracted from Garg and Balthasar [9] whereas IgG data in female 22-g nude mice were extracted form Baxter et al. [4] In total, there were 1488 individual data points as included in the Supplementary file XFit_DataV7_1000h.mat.

The data was split into a training and validation datasets, as summarised in Table 1.

Non-compartmental analysis

A non-compartmental analysis (NCA) of blood DMS5558, albumin, and hIgG1 data in rats and mice was performed using Matlab™ 2017a/SimBiology™ v5.6 (Mathworks,

Cambridge, UK). The plasma half-life of the AlbudAbs™ in blood were taken from previous PK analyses (unpublished GSK data).

General PBPK model description

The PBPK model includes lungs, lumped lymph node, heart, lumped gastrointestinal tract, liver, spleen, pancreas, muscle, skin, bone, brain, thymus, adipose and kidney as shown in Fig. 1. These organs account for about 98% of the body and the balance is represented by 'other' to make up for total body volume and blood flow rate. Peripheral plasma is represented by the arterial compartment. All organs contain vascular, interstitial and endosomal compartments, as shown in Fig. 2. All modalities, except DMS5558 dAb2 and free DMS5538, were subject to FcRn-mediated recycling and transcytosis in the endosomal compartment as shown on Supplementary Fig. 1.

In addition, some organs are further modified to capture their specific physiological features. The kidneys are supplemented by a lumped compartment containing the Bowman's capsule and loops of Henle (BCLH), like in our previous model [12]. Also, the brain interstitial space has been supplemented with cerebrospinal fluid (CSF) flow which empties into the central circulation, whilst the lung contains an alveolar compartment. Unlike previous models by us and others, at the exception of Meno-Tetang et al. [18], we also included the blood supply to lymph nodes [19, 20].

All soluble plasma proteins are subject to macropinocytosis into endosomal space, as modelled by Garg and Balthasar [14], where albumin and IgG can reversibly bind to FcRn. The unbound endosomal proteins are subject to non-specific degradation, while the FcRn-bound fraction is subject to recycling into extracellular space.

The solute exchange between vascular and interstitial compartments is described by the two-pore model and includes net and isogravimetric lymph flows J_{org} and $J_{org.ISO}$ for filtration and permeability-surface area product (PS_{org}) for diffusion as defined by us previously [12] and outlined in Fig. 2 and in detail for the kidneys and the brain in the Supplementary Fig. 1. The differential equations driving those exchanges are provided in the supplementary materials.

PBPK model parameters

All fixed parameter values in the PBPK model are listed in Table 2 in three categories: physiological parameters, endosomal parameters and two-pores extravasation parameters.

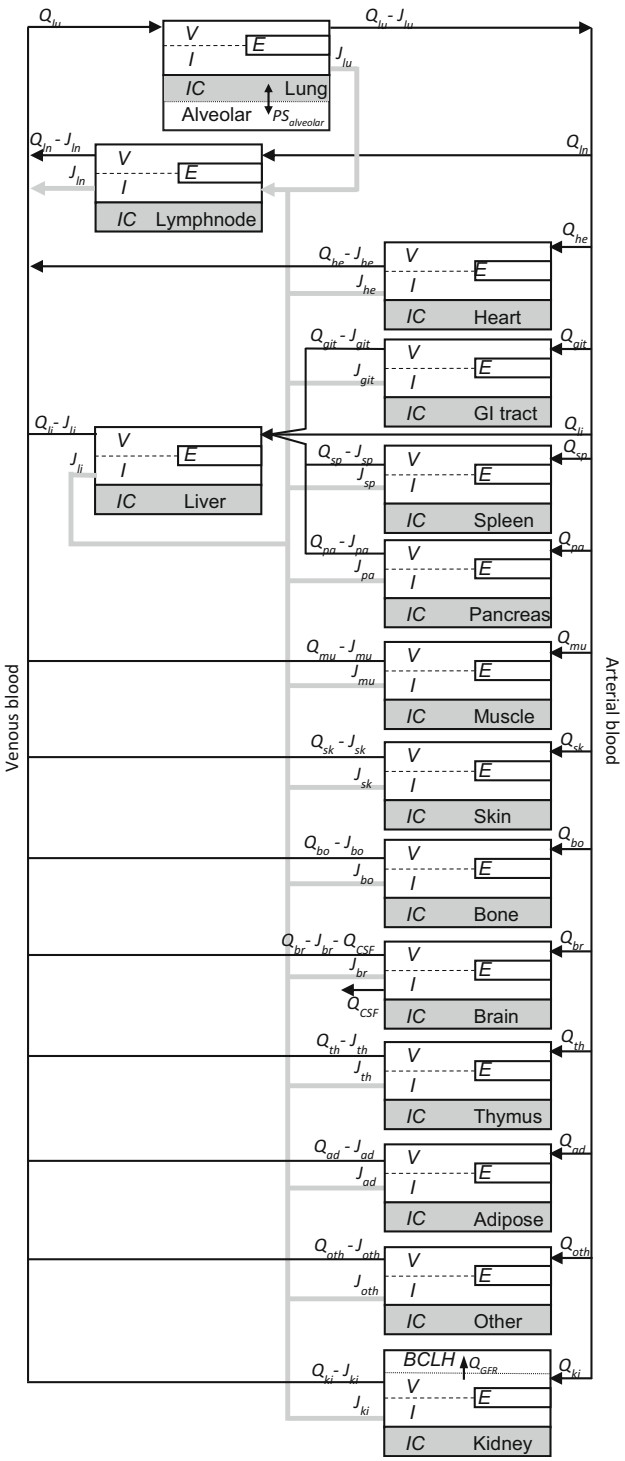

Fig. 1 Structure of the whole body PBPK. All organs are represented by a compartment connected with plasma flow rate (Q_{org}, black line) and lymph flow rate (J_{org}, gray line) and they are further divides into vascular space (V), interstitial space (I), intracellular space (IC) and endosomal space (E). *lu* lung, *ln* lymphnode, *he* heart, *git* GI tract, *li* liver, *sp* spleen, *pa* pancreas, *mu* skeletal muscle, *sk* skin, *bo* bone, *br* brain, *th* thymus, *ad* adipose, *ot* other, *ki* kidney

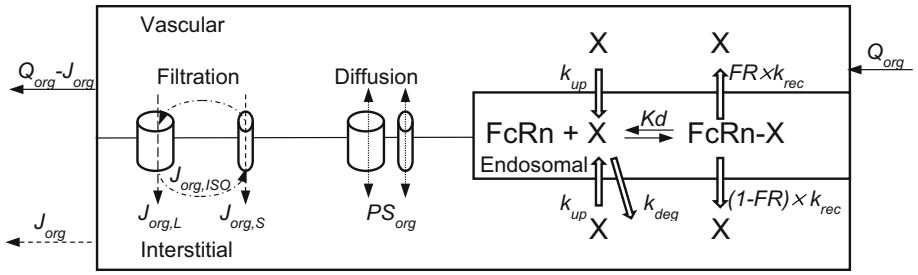

Fig. 2 Diagram showing fluid transfer from the vascular space to the interstitial space through small and large pores according to the two-pore hypothesis and the catabolism FcRn-mediated recycling in the endosomal space. Parameters values used are listed in Table 2, extravasation processes are denoted by dotted arrows, endosomal uptake, recycling and degradation are denoted by thick arrows, X illustrates any protein

Physiological parameters

We evaluated two alternative physiological parameter sets for mice and rats in our work. Set *SB* (Supplementary file *XFit_FullSystem_v13_SB.xlsx* and Supplementary Fig. 2) contains organ vascular space (capillaries) and interstitial space volumes from Shah and Betts [17], which are largely based on those of Graf et al. [21]. Set *BM* contains the organ vascular and interstitial volumes reported by Boswell et al. [22] (Supplementary file *XFit_FullSystem_v13_BM.xlsx* and Supplementary Fig. 2). Most of the respective parameter values in these two sets are closely correlated, except for skin and muscle, as shown on Supplementary Fig. 2. Total organ volumes and plasma flow rates were the same in both sets and taken from [17].

Peripheral plasma volume (i.e. veins and arteries) was defined as the difference between the total plasma volume (distributed between organ vascular spaces, veins and arteries) and the sum of organ vascular volumes. For the interstitial volumes, two options were considered in the PBPK model: option one assumes that the whole interstitial space is available to all modalities, while in option two the large molecules like albumin or mAbs could only reach 50% of the interstitial space available, as found by Wiig et al. [23]. Both parameter sets were supplemented with the capillary vascular volume and plasma flow rate of the lymph node, extracted from literature for the mice [19], and scaled up allometrically from mice to rats. Whilst standard endogenous plasma IgG levels where used throughout, in the case of mice raised in germ free conditions the level of circulating antibody can be expected to be 10- to 20-fold lower according to Bos et al. [24]. This can be expected to result in higher free FcRn concentration available for IgG recycling and its slower clearance, as revealed by the approximately 450-h terminal half-life of 7E3 mouse IgG [14] in mice.

Endosomal parameters

FcRn was assumed to reside only in the endosomal compartment, with a volume fixed at 0.5% of that of total tissue as in [14, 15, 17].

Two independent endosomal FcRn concentration values from literature were tested in the PBPK model. The low value of 9 µM was calculated by averaging FcRn tissue concentrations as measured by Fan et al. using mass spectrometry [25] and scaled to 0.5% endosomal compartment volume fraction. The high value of 266 µM was based on the results from Western blotting of HepG2 cells by D'Hooge et al. [26] and qPCR of mouse tissues by Chen and Balthasar [27].

The interactions of albumin with FcRn are known to follow 1:1 stoichiometry [28]. The dissociation constants for albumin binding to FcRn ($K_{d,albumin:FcRn}$) was obtained from Cameron et al. [29].

Since an IgG molecule binds to two FcRn molecules as described by Abdiche et al. [26], its effective affinity in vivo ($K_{d,IgG:FcRn\,1:2}$) is expressed as a function of the intrinsic affinity for 1:1 interaction determined in vitro ($K_{d,IgG:FcRn\,1:1}$) and its *avidity* as shown in Eq. 1 for mouse IgG in mouse, as described in Eq. 2.

$$K_{d\,mouse\,IgG:FcRn\,1:2} = \frac{K_{d\,mouse\,IgG:FcRn\,1:1}}{avidity} \tag{1}$$

The values of $K_{d,IgG:FcRn\,1:1}$ measured by Abdiche et al. [40] were tenfold lower for human IgG1 compared to mouse IgG1.

$$\frac{K_{d\,human\,IgG:FcRn\,1:1}}{K_{d\,mouse\,IgG:FcRn\,1:1}} = \frac{164nM}{1902nM} \sim \frac{1}{10} \tag{2}$$

Abdiche et al. also compared mouse PK profiles for a panel of human IgG1 variants and showed that monovalent IgG heterodimers (1 functional FcRn-binding site) cleared significantly faster than their corresponding homodimers (2 functional FcRn-binding sites). Interestingly, the plasma half-life derived from the monovalent human IgG1 variant

Table 2 PBPK parameters fixed in the model

Parameter (unit)	Description	Value in mice	Value in rats	References
Physiological parameters				
[Albumin] (M)	Endogenous albumin plasma concentration	3.4E−4	5.4E−4	[36, 37]
[IgG] (M)	Endogenous IgG plasma concentration	2.6E−5[a]	4.5E−5	[36, 37]
BCLH (%)	Fractional renal volume of the combined compartment of BCLH	9.5		Estimated in [12]
Q_{lnd} (ml/h)	Plasma flow rate of the lymph node	1.65	16.5	For mouse [38, 39]. For rat linear scale with body weight.
Θ	Glomerular filtration coefficient	Variable		cf. Supplementary Material
Endosomal parameters				
$V_{endosomal}$ (%)	Fractional volume of endosomal compartment	0.5%		[14]
FcRn low (M)	Endosomal FcRn low concentration	9.1E−6		[25]
FcRn high (M)	Endosomal FcRn high concentration	2.66E−4		[27]
$Kd_{albumin:DMS5558}$ (M)	Albumin affinity for DMS5558	1.30E−7	6.10E−7	GSK data
$K_{d,albumin:FcRn\ 1:1}$ (M)	FcRn affinity for albumin	7.6E−7	3.5E−6	[29]
$K_{d,IgG:FcRn\ 1:1}$ (M)	FcRn monovalent affinity for IgG	1.90E−6	1.35E−7	[40]
Avidity	FcRn avidity for IgG	10		Derived from [26]
k_{up} (1/h)	Non-specific protein uptake rate constant from extra-cellular into endosomal space	0.9		Derived from Eq. 4.
Two-pore extravasation parameters				
a_e (nm)	Protein stokes radius	Variable		Calculated from the molecular weight [12]
r_L (nm)	Default large pore radius	22.85		[41]
$r_{L,li}$ (nm)	Liver large pore radius	105		[42]
$r_{L,bo}$ (nm)	Bone large pore radius	105		Assumed the same as in liver
$r_{L,sp}$ (nm)	Spleen large pore radius	105		Assumed the same as in liver
$r_{L,ki}$ (nm)	Kidney large pore radius	12.5		[16, 21, 41]
$r_{L,git}$ (nm)	GI tract large pore radius	33.5		[16, 21, 41]
$r_{L,pa}$ (nm)	Pancreas large pore radius	26.5		[16, 21, 41]
r_S (nm)	Default small pore radius	4.4		[41]
$r_{S,gi}$ (nm)	GI tract small pore radius	5		[16, 21, 41]
α_L	Default large pore hydraulic conductance	0.05		[12]
$\alpha_{L,li}$ (dimensionless)	Liver large pore hydraulic conductance	0.07		[12]
$\alpha_{L,bo}$ (dimensionless)	Bone large pore hydraulic conductance	0.07		Assumed the same as in liver
$\alpha_{L,sp}$ (dimensionless)	Spleen large pore hydraulic conductance	0.07		Assumed the same as in liver
$\alpha_{L,lu}$ (dimensionless)	Lung large pore conductance	0.07		[16, 21, 41]
$\alpha_{L,mu}$ (dimensionless)	Muscle large pore conductance	0.035		[16, 21, 41]
$\alpha_{L,sk}$ (dimensionless)	Skin large pore conductance	0.035		[16, 21, 41]

BCLH Bowman's Capsule and Loops of Henle

[a]For the data set from Garg et al. [14], tenfold lower level was used, given that those mice had an abnormally long half-life, potentially due to a germ free environment (Bos et al. [24])

Small pore hydraulic conductance = 1 − large pore hydraulic conductance

was very close to the typical plasma half-life of a wild-type mouse IgG1.

As similar half-lives imply similar in vivo IgG–FcRn binding, the *avidity* for mouse IgG1 in mouse was calculated to be 10 based on Eq. 3.

$$\frac{1}{avidity} = \frac{K_{d\ mouse\ IgG:FcRn\ 1:2}}{K_{d\ mouse\ IgG:FcRn\ 1:1}} = \frac{K_{d\ human\ IgG:FcRn\ 1:1}}{K_{d\ mouse\ IgG:FcRn\ 1:1}} \sim \frac{1}{10} \tag{3}$$

Non-specific uptake of proteins from extracellular space into the endosomal compartment was characterized by the parameter k_{up}, which was calculated from Eq. 4. It was assumed that k_{up} was conserved across species and was the same for all modalities.

$$k_{up} = \frac{0.693 \times V_{ss} \times d}{0.005 \times t_{1/2}} \tag{4}$$

where d is the tissue density (assumed to be 1 g/ml), V_{ss} (assumed to be 0.13 mL/g as determined by NCA, see Supplementary Table 1) is the typical volume of distribution of large molecule like albumin and IgG at steady state and $t_{1/2}$ is the half-life of albumin and IgG in mice in the absence of FcRn-mediated recycling (assumed to be 20 h) [30–34].

The recycling first-order rate constant for albumin ($k_{rec,albumin}$) was estimated by the PBPK model. Since IgG binds two FcRn molecules at the same time [26], its recycling constant ($k_{rec,IgG}$) was fixed to $0.5 \times k_{rec,albumin}$.

The degradation first-order rate constant for all modalities not bound to FcRn in the endosomal compartment (k_{deg}) was derived from the observation by Kim et al. [35] that in mice the amount of albumin degraded was equal to the amount of albumin recycled, (cf. Eq. 5).

$$k_{deg} \times [Albumin]_{free.endosome} = k_{rec,albumin} \times [Albumin - FcRn]_{Complex.endosome} \tag{5}$$

where the endosomal concentration values for free and FcRn-complexed albumin were estimated from the steady state of the best fit BPPK variant model. The degradation rate constant and the recycling rate constant were assumed to be conserved across species.

Two-pore extravasation parameters

Default parameters associated with the extravasation were taken from our previous model [12], which assumes the same large and small pore sizes and ratios for lymph nodes, heart, muscle, brain, thymus, adipose and others. We implemented organ-specific large to small pore ratios and sizes for the rest of the organs, to reflect the experimentally observed variation in vascular permeability between organs as reported in Table 2 and Supplementary Materials.

Glomerular filtration coefficient Θ for different modalities and proteins was calculated from an empirical equation as function of the hydrodynamic radius and it is provided in the differential equations from the Supplementary materials.

PBPK model optimisation

PBPK parameters were optimized by fitting simultaneously all blood and tissue concentration–time data from the training dataset (DMS5558, dosed albumin and dosed IgG1 in mice and rats). Each model optimisation run included two phases: (i) the baseline phase (arbitrarily set from time 0 to 1000 h), to enable the interstitial and endosomal concentrations of endogenous albumin and IgG to reach steady state as initial conditions and (ii) the dosing phase, where the dosing event was triggered, and the tissue concentration time course was obtained. Using this two-steps process, endogenous albumin and IgG determined the level of free FcRn available for the dosed proteins, as well as their own steady-state concentrations in interstitial and endosomal compartments. A total of fourteen parameters were fitted simultaneously across the training data sets from both species: organ-specific ratios of lymph and plasma flow rates (J_{org}/Q_{org}) and endosomal recycling constant for albumin $k_{rec,albumin}$.

Separate model variants for mice and rats with appropriate physiological parameters were used according to the species origin of the data set. Customised mouse physiological parameter set variants were used for mIgG1 (7E3) data in mice with low endogenous IgG [14] and for residualizing ^{111}In-labelled MOPC21 IgG data [9].

PBPK model variants selection

Two best fit PBPK model variants based on *SB* or *BM* physiological parameters set were selected based on the Akaike information criterion (AIC) [43]. FcRn concentration (9 μM or 266 μM) and the available distribution volume for larger proteins (adjusted to 50% or 100% of the interstitial volume of the organ) were considered across the PBPK model variants. A sensitivity analysis was performed by calculating the mean square error (MSE) after increasing or decreasing the best fit parameter values one by one, by a factor of two. The robustness of the final global fit was probed by refitting the data using initial parameter values all randomly and simultaneously displaced two- or tenfold from their respective best fit values.

Model evaluation

The best fit variants for each set of physiological parameter sets were further evaluated using the validation dataset.

Table 3 PBPK model variant selection

Physiological parameter set	Variants	Interstitial volume for albumin and IgG (% of interstitial space)	FcRn concentration (μM)	AIC
SB	***1.SB***	**50%**	**9**	**10482**
Shah and Betts [21]	*2.SB*	100%	9	10502
	3.SB	50%	266	10801
BM	*1.BM*	50%	9	10844
Boswell et al. [22]	***2.BM***	**100%**	**9**	**10754**
	3.BM	50%	266	11224

The best fit variant for each parameter set is in bold

Firstly, tissue distribution time course for mIgG1 in FcRn knock-out (KO) mice as reported by Garg and Balthasar [14] were predicted by turning off the FcRn-binding activity in the model and compared with the literature data. Secondly, the tissue distribution time course of DMS5538 was predicted and compared graphically to the observations in mice and rats. Finally, the blood PK profiles of the AlbudAbs™ in mice with different affinities for albumin were predicted. For each predicted profile, a half-life value was derived and compared to the observed half-lives obtained by previous PK analyses.

Software

Matlab™ R2017a and SimBiology™ version 5.6 were used to build the PBPK model and perform data analysis. The script *PBPKassembler.m* (Supplementary Material) assembles the full SimBiology™-compliant PBPK model by replicating the compartments and their contents, as outlined in Supplementary Fig. 3. The script then adds the intercompartmental reactions by flow or two-pore exchange and generates all the relevant parameters and rules as defined in SimBiology™ and modifies individual organ modules further for kidneys and the brain to capture the respective unique organ-specific physiological features.

Non-linear least squares fitting of the experimental data to the PBPK model was performed in Matlab™ based on the Matlab™ *nlinfit* function with predictions for each experimental data point generated using *sbiosimulate* function. The custom script *XFitModel_v8_Par_1000h.m* is provided as supplementary material. The half-life predictions for AlbudAbs™ of different affinities was done on simulated concentration time course in blood.

Results

PBPK variant model selection

The compiled PBPK model structure using either of the two physiological parameter sets *SB* and *BM* containing 70 compartments (organs and sub-compartments), 636 molecular species (free and bounds modalities in different organs and sub-compartments), 1210 reactions and fluxes (between modalities in different compartments), 2154 rules (e.g. types of pores, endosomal variables) and 2244 parameters (modality specific and organ specific). Of the latter, there are 89 physiological parameters (organ total, plasma and interstitial volumes, plasma flow rate, FcRn binding affinities, endogenous albumin and IgG concentrations etc.) and 48 two-pore parameters (small and large pore radius and large pore relative hydraulic conductance). The rest of the parameters are modality, two-pore extravasation and model-related parameters derived from the above and the hydrodynamic size of the protein or complex in circulation.

The performance of the six model variants is summarised in Table 3. The AIC values indicate that in all scenarios, the *SB* physiological parameter set allowed better overall description of the data. Within parameter set *SB*, the variant 1.*SB* with the lowest FcRn concentration and with the distribution volume for albumin and IgG restricted to 50% of the interstitial space produced the best results. Within parameter set *BM,* the variant 2.*BM* with the lowest FcRn concentration and albumin and IgG allowed to distribute in the entire interstitial space produced the best results.

The concentration–time profiles of dAb2, albumin and the IgG in all mice organs are displayed in Fig. 3 for the two best performing variant 1.*SB* (black line) and 2.*BM* (red line). The plots for the rat data are shown in Supplementary Fig. 4.

Fig. 3 Globally fitted concentration–time time profiles of ^{3}H-DMS5558 dAb2 by QWBA (**a**), ^{3}H-MSA by QWBA (**b**), ^{125}I-IgG1 in mice from Garg [14] (**c**), **d**: ^{111}In-IgG1 in normal mice [9] from PBPK model variants. In black are the predictions from 1.SB variant, in red those based on 2.BM variant (Color figure online)

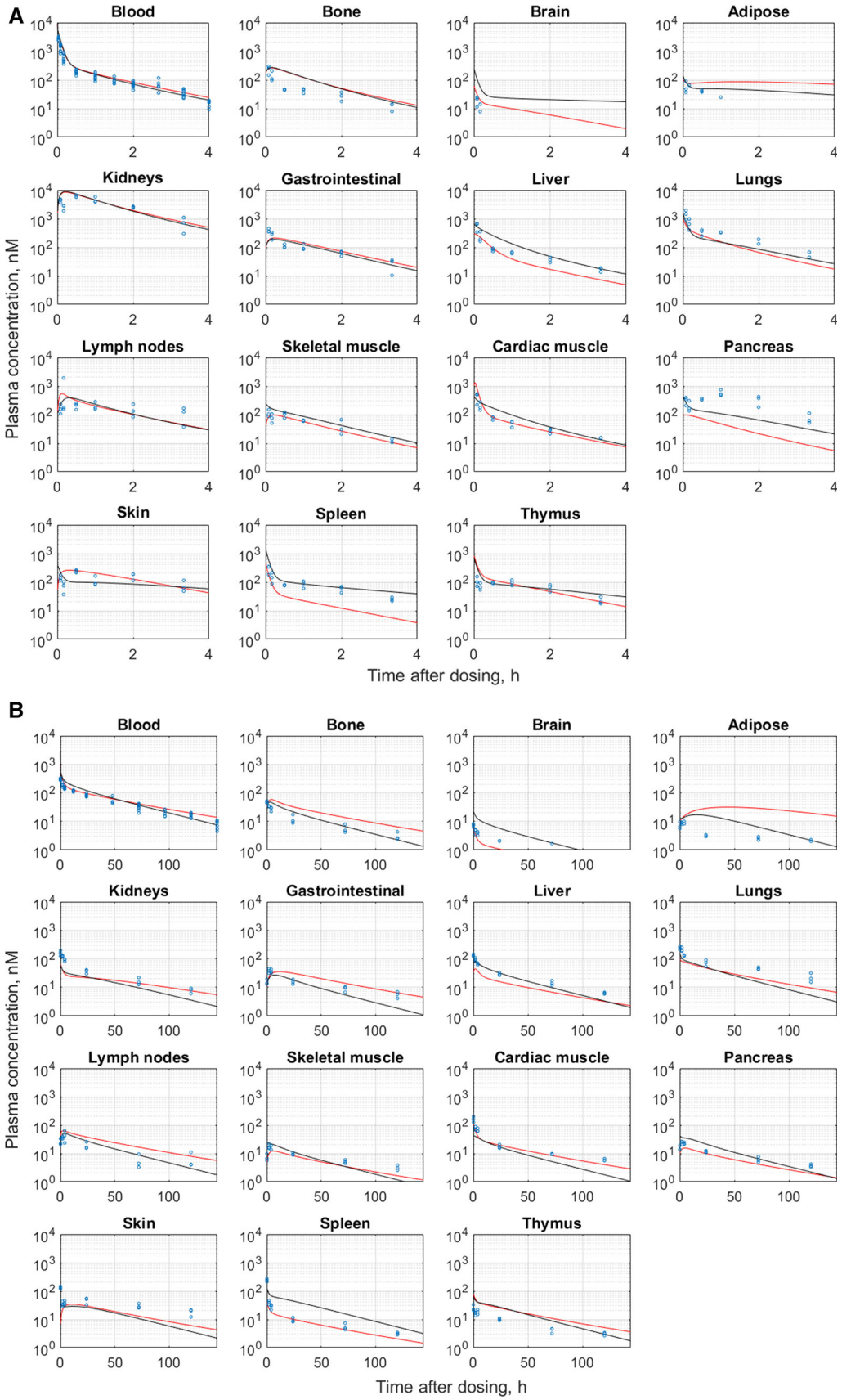
A
Blood
Bone
Brain
Adipose
Kidneys
Gastrointestinal
Liver
Lungs
Lymph nodes
Skeletal muscle
Cardiac muscle
Pancreas
Skin
Spleen
Thymus
Plasma concentration, nM
Time after dosing, h
B
Blood
Bone
Brain
Adipose
Kidneys
Gastrointestinal
Liver
Lungs
Lymph nodes
Skeletal muscle
Cardiac muscle
Pancreas
Skin
Spleen
Thymus
Plasma concentration, nM
Time after dosing, h

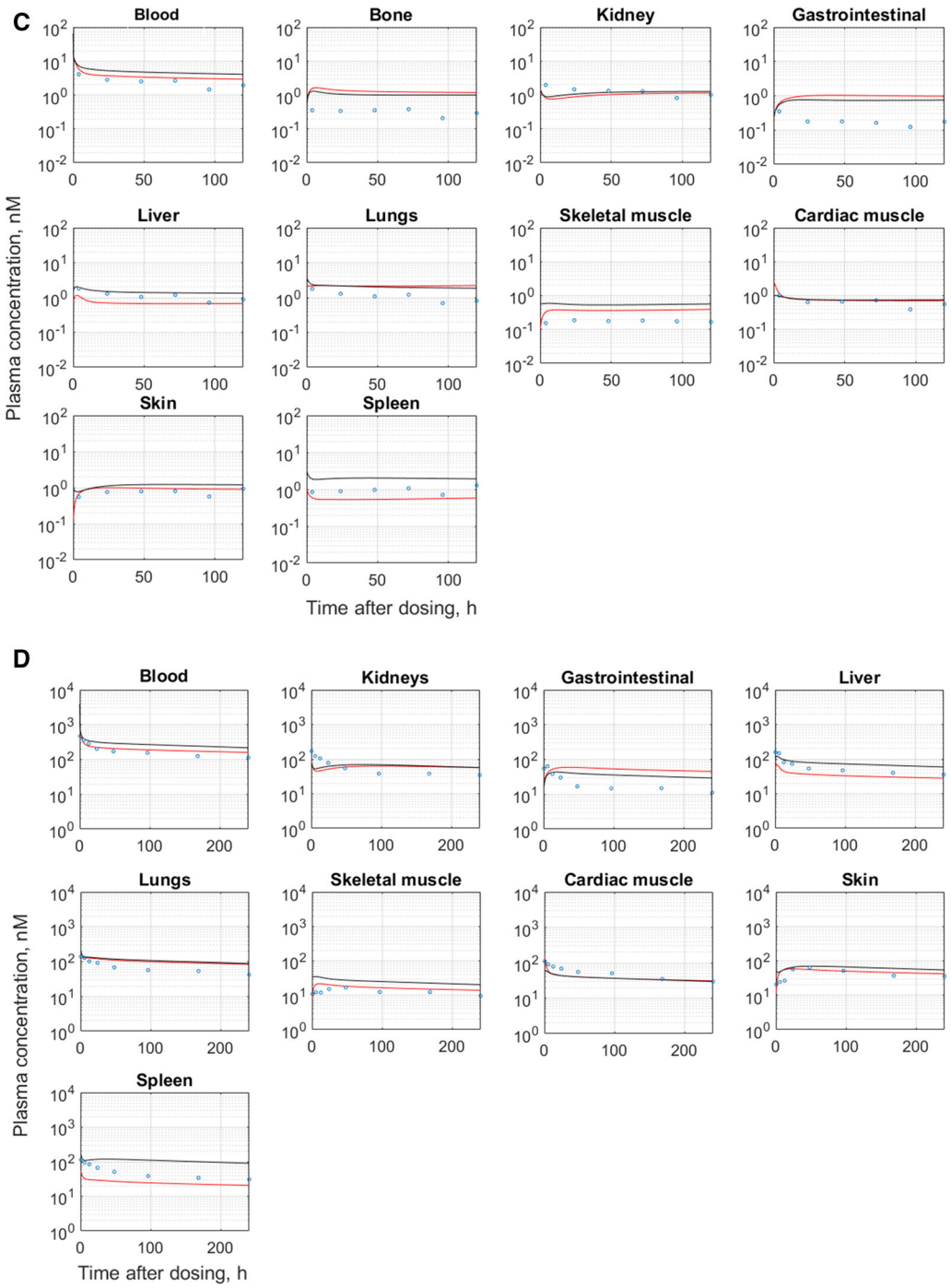

Fig. 3 continued

DMS5558 dAb2 in mice

DMS5558 dAb2 in mice (Fig. 3a) follows similar biphasic disposition profiles in blood for both physiological data sets, with a short distribution phase lasting less than an hour, followed by a rapid elimination phase with half-life of less than an hour. Similar profiles were observed in liver, lung, cardiac muscles, thymus and spleen, and gastrointestinal tract whereas a slower uptake and a monophasic disposition was found in bone marrow, lymph nodes,

Table 4 Estimated lymph flow fractions of the respective organ plasma flow rate (Jorg/Qorg) and first-order recycling rate constant (krec, albumin) from model variants 1.SB and 2.BM

Parameter	Organs	Variant 1.*SB*	%RMSE	Variant 2.*BM*	%RMSE
Fractional organ-specific lymph flow rates	Heart	1.32E−04	24	4.37E−03	34
J_{org}/Q_{org} ratio	Lung	6.72E−06	36	1.84E−05	39
	Muscle	2.41E−03	15	2.14E−03	16
	Skin	1.67E−03	18	7.83E−03	13
	Adipose	7.18E−04	20	6.03E−04	24
	Bone	7.28E−03	19	6.24E−03	19
	Liver	1.02E−02	26	6.58E−03	30
	GIT	4.17E−04	16	5.31E−04	17
	Pancreas	2.48E−04	26	2.20E−04	22
	Thymus	5.36E−05	29	1.12E−0l4	24
	Kidney	1.82E−05	43	1.07E−04	95
	Brain	5.70E−05	36	5.84E−05	56
	Spleen	8.40E−05	31	3.05E−05	71
	Other	2.5E−04	Fixed	5.3E−04	Fixed
	Lymph nodes	2.5E−04	Fixed	5.3E−04	Fixed
$k_{rec,albumin}$ 1/h		23.37	0.26	23.36	0.29
MSE		0.459		0.5448	

The absolute values of plasma flow and lymph per organs (mL/h) are in Supplementary Table 3, including the values calculated by Eigenmann et al. [44] and Niederalt et al. [13]

k_{rec} recycling rate constant, *RMSE* root mean square error representing the uncertainty of the estimated parameter, *MSE* mean square error, representing the goodness of the overall PBPK fit across all modalities and species at the same time

skeletal muscle, pancreas and skin. The model predictions diverged more in the case of brain and spleen. The model captures well the considerably high accumulation of dAb2 in the kidney. In adipose tissue, the model underestimates the elimination of dAb2 whilst in the pancreas, the trend of the observed data is not captured. Similar observations were made for DMS5558 in rats where good to satisfactory fit between data and the model was also observed in adipose tissue and pancreas (Supplementary Fig. 4A).

Albumin in mice (Fig. 3b)

Both physiological parameter sets used in our PBPK model yielded similar tissue concentration–time course predictions with the distribution, lasting about 10 h in blood, which was followed by a slower terminal elimination phase. The rest of the tissue profiles followed a similar pattern with skeletal muscle, skin, lymph nodes, spleen, thymus, and even gastrointestinal tract displaying accumulation of albumin during the distribution phase, while lung, liver, bone marrow, pancreas and cardiac muscle closely follow the blood concentration time course. The model does not predict an accumulation of albumin in the kidney, which agrees with observations. In brain, the concentrations remain low. In rats, the tissue concentration time profiles were very similar for both physiological parameter sets, with only blood concentrations slightly underestimated (Supplementary Fig. 4B).

IgG1 in mice (Fig. 3c, d)

The tissue distribution time course profiles of IgG1 were similar to those of albumin. The relatively fast decrease in plasma concentration during the distribution phase lasted for about 15–20 h and was followed by slow terminal elimination. Similar overall profiles were observed in most tissues except skeletal muscle and skin, where moderate accumulation took place during the distribution phase instead. The model performs similarly to describe the rat data across both data sets, although brain is better captured with parameter set *SB* (Supplementary Fig. 4C). The examples of full body cross-sections for mice and rats are shown on Supplementary Fig. 5.

The net organ lymph flow rates expressed as a fraction of respective plasma flow values (J_{org}/Q_{org} ratio) and albumin recycling rate constant ($k_{rec,albumin}$) were estimated with good accuracy for both *1.SB* and *2.BM* model variants (Table 4). In addition, the residual error (MSE) for both

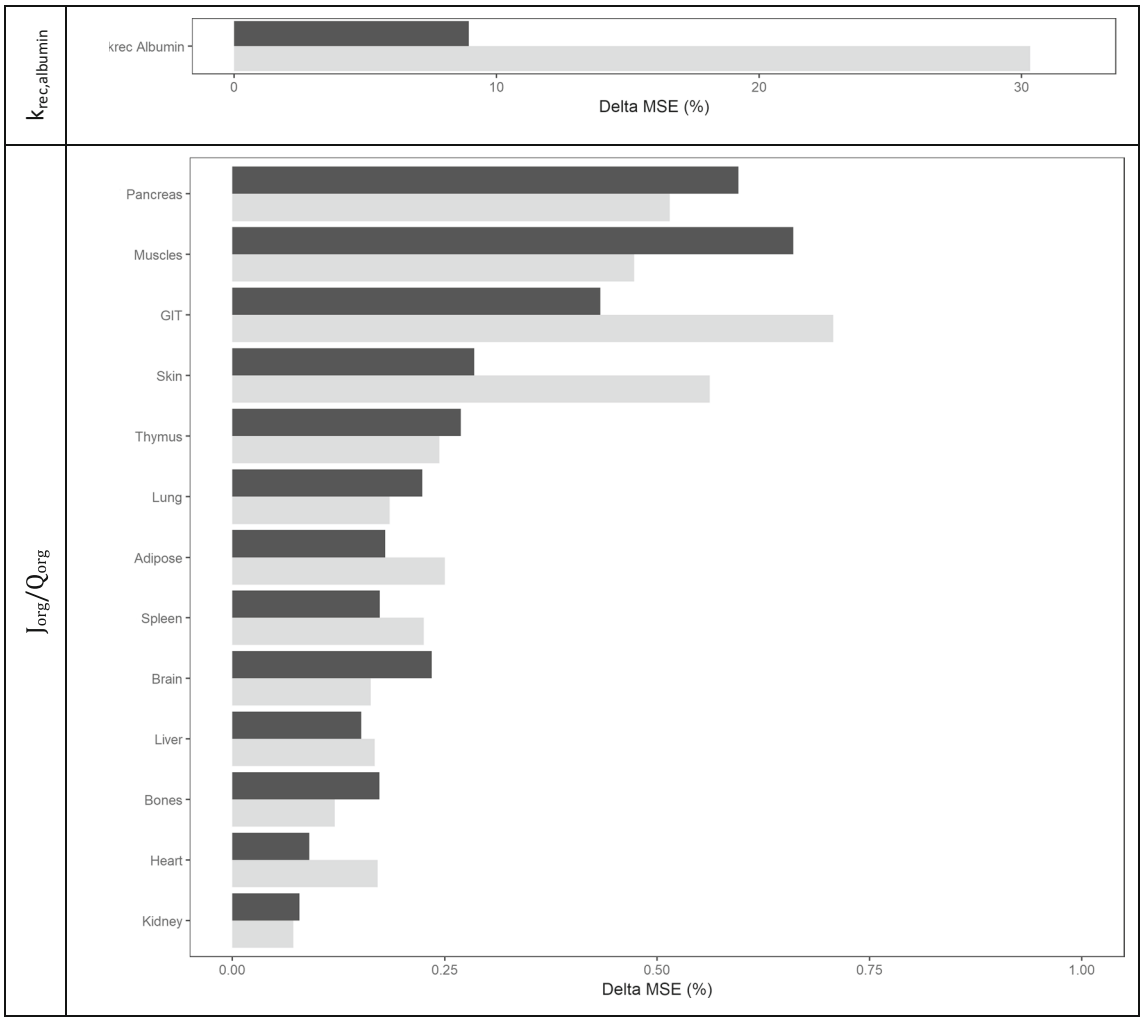

Fig. 4 Sensitivity analysis on delta MSE. PBPK parameter estimates from 1.SB ($k_{rec,albumin}$ and J_{org}/Q_{org} ratio) were increased (in black) or decreased (in gray) by a factor of 2. The recycling rate constant for albumin ($k_{rec,albumin}$) has been plotted on a different y scale from the J_{org}/Q_{org} ratio

variants was low and no cross-correlation was observed between parameter estimates (Supplementary Table 2). The parameter J_{org}/Q_{org} ratio for lymph nodes and the 'other' tissue were taken as the median value of all fitted organ values. Organ-specific lymph flow rates estimated from *1.SB* and *2.BM* differ no more than twofold, except for the heart where *1.SB* parameter yields 30-fold lower estimate than *2.BM*. Parameter estimates of J_{org}/Q_{org} vary significantly between organs, from about 0.0006% for the lung and brain to 1% for the liver and bone. The fractional extravasation lymph flow rate into the lymph nodes was defined as the median of all fitted tissues, just like the 'other' organ because J_{ln}/Q_{ln} was strongly cross-correlated with J_{org}/Q_{org} from other fitted organs. This is the consequence of any variation in J_{ln}/Q_{ln} can be offset with opposite change in any other organ J_{org}/Q_{org} value. The estimate of the first-order recycling rate constant for albumin ($k_{rec,albumin}$) was similar between the two physiological parameter variants of the model.

The results shown in Fig. 4 illustrate the PBPK model sensitivity analysis and demonstrate that changes (twofold increase or decrease) in estimated organ-specific lymph flow fractions (J_{org}/Q_{org}) always resulted in 0.1–0.8% increase in MSE values. In contrast, changes to the endosomal recycling constant for albumin $k_{rec,albumin}$ resulted in 10- to 30-fold higher perturbation and where more pronounced for the decreased value of the parameter.

The residual analysis of global fit is shown on Supplementary Fig. 8. There is generally good agreement between the observed and predicted concentration values spanning five orders of magnitude. The only systematic deviations are for the DMS5558 dAb2 rat brain data which were considerably higher than for the same compound in mice-albeit detected by different methods. In addition, lower than predicted ^{111}In-labelled MOPC21 mouse IgG

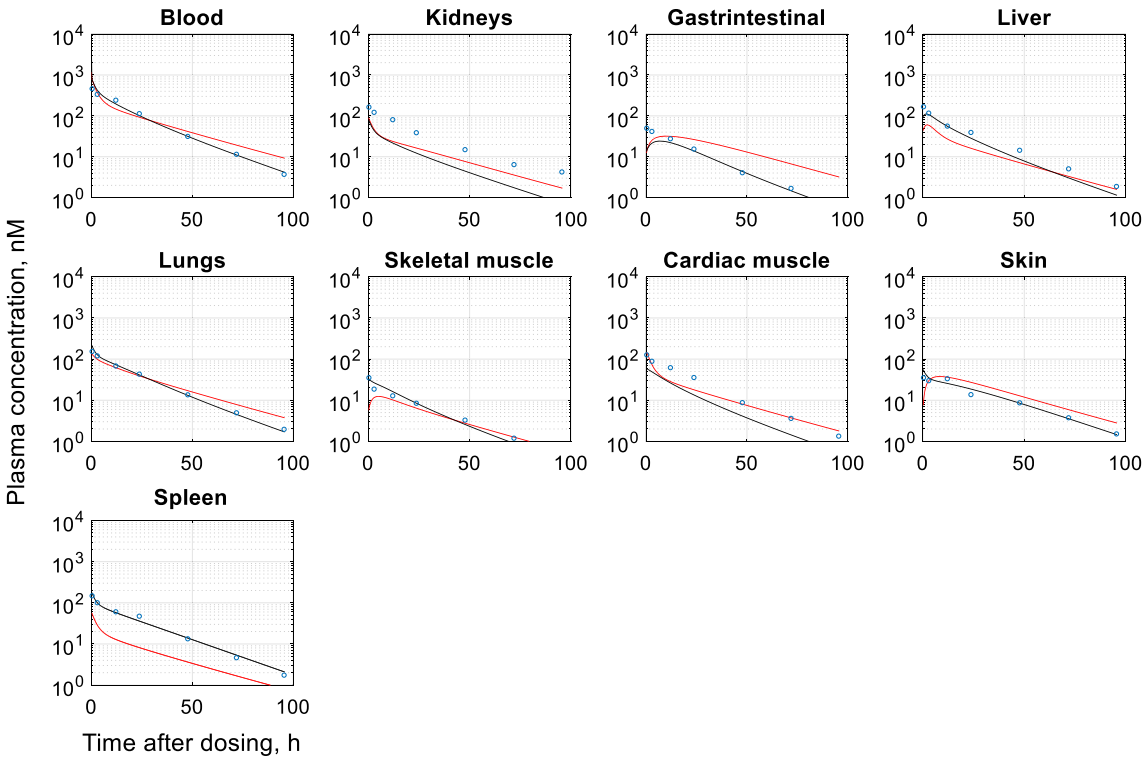

Fig. 5 IgG1 tissue distribution time course data in FcRn KO mice as reported by Garg and Balthasar [14]. In black are the predictions from 1.SB variant, in red those based on 2.BM variant (Color figure online)

data [9] suggests the possibility of incomplete residualization of the label or leaking from the chelator.

Robustness analysis

In the case of the initial values displaced by a factor of two from those achieved in the best fit, six out of ten runs ended with the same solution as the original fit *1.SB*. The remaining four runs ended at a substantially higher local MSE minimum which was characterized by 25-fold increased, but poorly defined value for $k_{rec,albumin}$ (RMSE = 400%). In the case of random displacement of the parameter initial values by a factor of ten, three out of ten runs ended at the starting values, two at the second minimum described above and three at two additional local minima at even higher MSE. Two runs failed to converge and ended with an integration error. Therefore, we concluded that in the parameter and data space solution *1.SB* may be the global minimum. The values for J_{org}/Q_{org} and $k_{rec.albumin}$ from the robustness analysis outcomes which converged in the same minimum are displayed in Supplementary Table 4.

Model evaluation

The PBPK model variants *1.SB* and *2.BM* were further evaluated using the validation dataset as described in the Methods section. Evaluation results based on data from FcRn knock out (KO) mice are shown in Fig. 5. The predictions closely matched the experimental observations, with *1.SB* providing slightly better fit than *2.BM*. There is no FcRn-mediated recycling in these animals while the renal filtration is negligible due to the size of the proteins. As a result, protein elimination kinetics is solely determined by the *Kup* value estimated from NCA data.

The evaluation results for the albumin-binding DMS5538 dAb2 are shown in Fig. 6 for the mouse and show a good agreement between the observations and the model predictions. The results obtained in rats were similar and shown on Supplementary Fig. 6.

In addition, the PBPK predictions of terminal half-lives for the AlbudAbs™ were similar to the experimentally measured values (GSK, unpublished data), capturing both the plateau for the high affinity AlbudAb™ clones and the accelerated clearance of those with low affinity. However, the variant *2.BM* was in better agreement with the data than *1.SB* (Fig. 7).

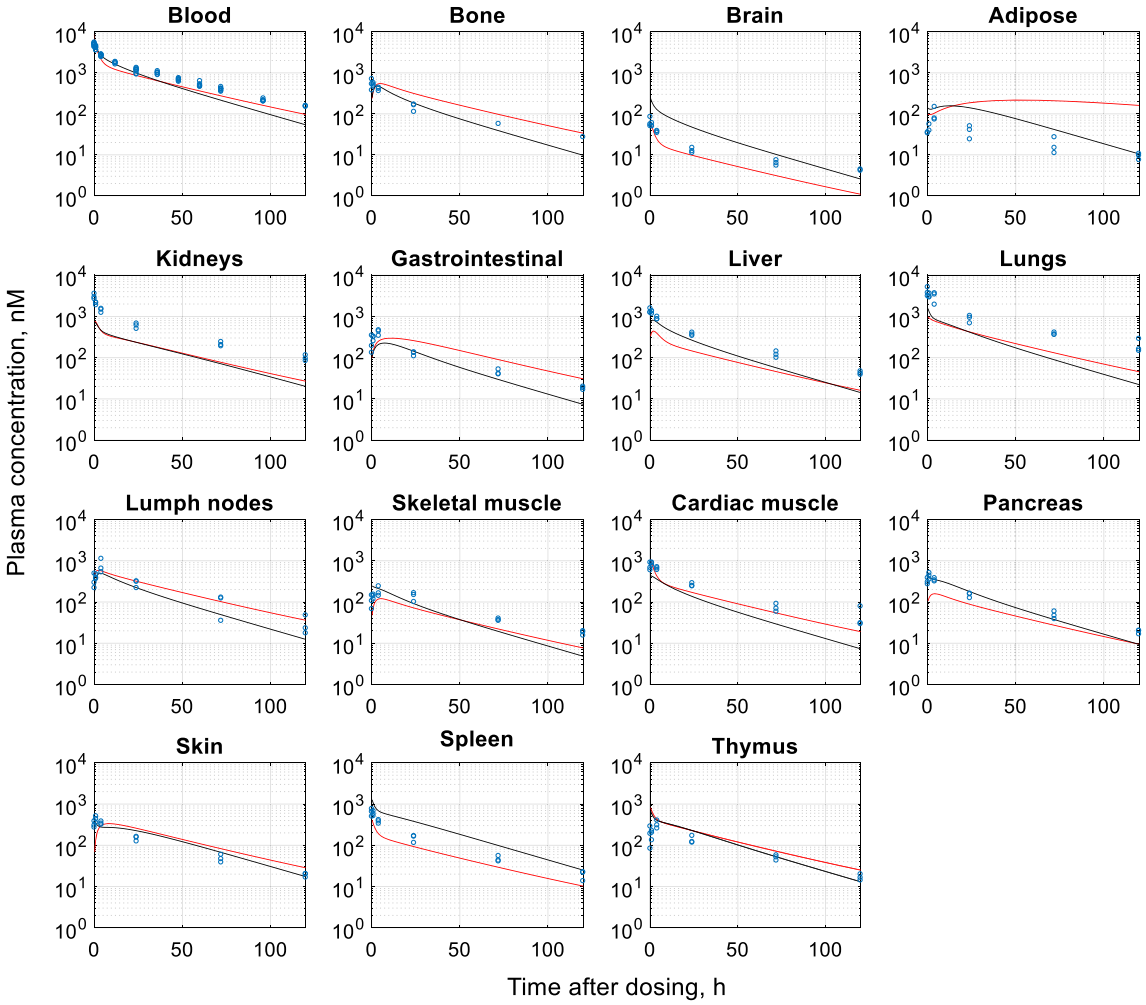

Fig. 6 Best fit 1.BS and 2.BM model predictions for 10 mg/kg albumin-binding dAb2 (DMS5538) tissue distribution time course in mice. In black are the predictions based on the physiological parameter set SB, in red those using the physiological parameter set BM (Color figure online)

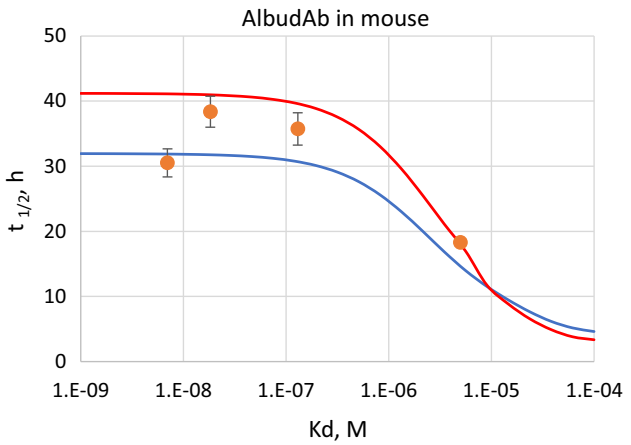

Fig. 7 Best fit 1.SB and 2.BM variants predictions and experimental observations for AlbudAb™ terminal half-life in mice as a function of affinity for albumin. In blue are the predictions 1.SB, in red those using the 2.BM. The time course data are shown on Supplementary Fig. 9

Discussion

PBPK for biologics has developed significantly since the first antibody-dedicated model was introduced by Covell et al. [45]. Cross-species PBPK models for mAbs have been developed by Shah and Betts [17], while Baxter et al. [9] and Ferl et al. [10] introduced the filtration-diffusion based two-pore model of Rippe and Haraldsson [16] to extend the approach to proteins of any size. However, in these models, the net and isogravimetric lymph flow were considered as independent parameters and the permeability-surface area product was assumed to be invariant for all organs, irrespective of vascular porosity. As a result, there was a large uncertainty and significant cross-correlation between parameter estimates, suggesting over parametrisation. In our previous paper [12], we addressed these issues by demonstrating that in the two-pore theory, the filtration and diffusion pathways are cross-correlated and a

single parameter, preferably organ-specific lymph flow, can be used to derive isogravimetric flow and PS product values. The same conclusion was independently reached by Gill et al. [11, 46] and Niederalt et al. [13] to describe tissue distribution and elimination kinetics of different human soluble proteins in different species, including humans. Although conceptually similar, the Niederalt model also explores the possibility of using experimentally measurable vascular hydraulic conductivity for calculating organ permeability-surface product area values, while empirically fitting fractional lymph flow values and coefficients $f_{Jiso,org}$ that link the isogravimetric and linear lymph flow rates across organs (with cross-species allosteric adjustment parameter). Interestingly, the mean $f_{Jiso,org}$ value fitted across tissues ($f_{Jiso,org} = 0.5 \pm 0.4$, range 0.01–0.96) is comparable with our two-pore model prediction which works out around 0.45 for most of the organs (range 0.3–0.7), suggesting close correlation between the models even when our described model uses one empirically fitted parameter (equivalent to $f_{lymph,org}$), while that of Niederalt [13] uses two ($f_{lymph,org}$ and $f_{Jiso,org}$).

In the PBPK model described in this manuscript, we expanded our previous approach by incorporating the endosomal compartment into all organs and used an extended dataset to cover a wide selection of proteins in rats and mice, including the FcRn-binding modalities like albumin and IgG. This model generated parameter estimates (i.e. J_{org}/Q_{org} ratio, $k_{rec,albumin}$) that can be applied across both species and across-modalities as well as derived parameters (e.g. $k_{rec,\ IgG}$, k_{deg}, J_{ISO}, PS).

PBPK model input

The species-specific vascular and interstitial compartment volume values can mostly be measured independently, as discussed in detail by Boswell et al. [22]. However, the reported values can occasionally show significant variation from one source to another. We, therefore, evaluated the impact of two sources of physiological parameters from Shah and Betts [17] (set *SB*) and Boswell et al. [22] (set *BM*) on the goodness of fit. The organ-specific interstitial volumes were quite similar between the two sets of physiological parameters. For vascular compartment volumes, the values for muscle and skin were significantly smaller in set *BM* than in set *SB* (Supplementary Fig. 2). Based on Figs. 3, 4, 5, and 6 and the AIC criteria from Table 4, the *SB* parameter set provided better overall fit to the experimental data. However, in muscles and skin, the set *BM* showed a closer fit to data during the distribution phase (see Fig. 3). Based on those observations, we decided to keep the two sets of physiological parameters in the PBPK model building process. To mitigate the variability in the physiological volume measurements from the literature, Eigenmann et al. [44] suggested that radiolabelled albumin could be more suitable for the quantification of vascular compartment volume than red blood cells and could more accurately predict the PK data of an IgG. This work, though limited to IgG, would merit to be further extend to other modalities. For information, the respective lymph flow estimates using the physiological values from Eigenmann et al. [44] and Niederalt et al. [13] are displayed on Supplementary Table 3, together with our own PBPK model estimates.

The interstitial space is understood to be filled with negatively charged proteoglycans [47], including fibres of collagen and elastin bathed in the interstitial fluid [48]. The structure of the interstitial matrix thus creates a gel-filtration-media like environment where the volume of distribution of a solute can depend on its size. This is in line with the observations of Wiig et al. [23] who found that only half of the interstitial space being available to small molecules can be reached by larger ones like albumin and IgG. Therefore, the effective available interstitial space may depend on the size of the protein and have an impact on the quality of the fit of the model to the data. The results were not unequivocal: the model variant *1.SB* provided a better fit with 50% available space, whereas the variant *2.BM* employed no interstitial volume restriction for protein distribution (cf. Table 4). Given that fit *1.SB* was significantly better than *2.BM*, it may be beneficial to consider protein size-dependent interstitial volume adjustments, although the implementation of such modality-specific compartment volumes can be computationally challenging.

FcRn [49] plays a key role in extending the plasma half-lives of IgG [31] and albumin [30]. At the mechanistic level, a complex network of proteins is involved, as reviewed by Scott et al. [50] and modelled by French and Lauffenburger [51]. However, we have implemented the simple one-compartment approximation introduced by Garg and Balthasar [14], which describes the non-specific uptake of IgG from the surrounding medium by micropinocytosis followed by reversible binding to FcRn in the endosomal space. The free fraction is then degraded whilst the IgG bound to FcRn is recycled. There is no FcRn turnover in the model, it resides only in endosomal space and the total amount present is constant. Given that our model also incorporates endogenous albumin and IgG, it is important to notice that FcRn is therefore defined as the total amount present, unlike the free fraction used more frequently when the endogenous IgG is not incorporated [9, 10, 17]. Recently, the relative FcRn tissue distribution and its absolute concentration was observed to be well-conserved across species, including Tg32 human FcRn transgenic mice according to Sari et al. [52]. However, FcRn total concentration is less well determined. Fan et al.

[25, 53] found using mass spectrometry in Tg32 mice that the total FcRn concentration ranged from 9 pmol/g in brain to 111 pmol/g in lymph nodes, with a weighed total average of 45 pmol/g (9 μM in the endosomal compartment if the volume of the latter is taken as 0.5% of that of total tissue as in references [14, 17]). Similar results were obtained by Wiśniewski et al. [54] who measured FcRn making up 0.00182% of total cell protein which translates to about 100 nM total cellular concentration and 20 μM in the endosomal compartment. On the other hand, around 15- to 30-fold higher levels have been estimated in HepG2 cells by western blotting by D'Hooghe et al. [26] or PBPK curve fitting [15, 27]. Based on those observations, we evaluated the goodness of fit obtained with either the low or the high estimates for FcRn concentration (9 and 266 μM). The lower estimate of 9 μM total endosomal FcRn provided a significantly better overall fit within both parameter sets used, as judged by the AIC criterion (see Table 4).

PBPK model outcomes: goodness of fits

There was a good agreement between the observations and PBPK predictions in blood across modalities and the plasma half-lives derived from the profiles using NCA were in line with literature values (cf. Supplementary Table 1). For example, the terminal plasma half-life of dAb was estimated to be < 1 h, in line with the expected rapid loss from the circulation [6]. The terminal plasma half-life of albumin was estimated at 35 h in mice which in line with Chaudhury et al. and Nolte et al. [30, 34] and 49 h in rats, close to 46 h reported by Gaizutis et al. [55]. The terminal half-life of GSK679586 hIgG1 in rats extends to 178 h, attributable to stronger binding of human mAb Fc region with rodent FcRn [26]. The model performance on the mouse data was good to satisfactory, except in pancreas and bone marrow, where more significant deviations were found. These organs are characterized by discontinuous vasculature [56], where the two-pore approach may not be the most appropriate. However, we cannot exclude experimental bias, since the fits are better in the case of rat data, when QRA instead of QWBA was employed for the quantification of tissue concentrations (Fig. 3 versus Supplementary Fig. 4).

If we compare the goodness of fits of the IgG in wild type mouse (Fig. 3c) with the one from Shah and Betts in the same species [17], there is no clear difference and both PBPK variants appear to predict the data well. This is not surprising, given that in the case of two-pore model the extravasation of larger proteins, like IgG, is predominantly filtration-driven, just like in the platform model of Shah and Betts [17]. The difference is expected to be more important in the case of smaller proteins, when diffusion becomes the dominant mode of transport.

PBPK model outcomes: parameter estimates

The total lymph flow rates calculated from the J_{org}/Q_{org} parameter estimates as a fraction of cardiac plasma flow were 0.14% in mice and 0.13% in rats for the selected *1.SB* variant model and 0.21% in mice and 0.18% in rats for the *2.BM* variant model (see Supplementary Table 3). There is only a limited amount of experimental data available for organ lymph flow rates but in humans the aggregate reaches 0.05–0.1% of cardiac plasma output [47, 57] which is close to the values we estimate for mice and rats. Many options are available for scaling organ-specific lymph flow rates from one species to another. The current PBPK model postulates conservation of lymph flow as a fraction of plasma flow as used by Shah and Betts [17] but scaling with organ volume has also been applied by Ferl et al. and Sepp et al. [10, 12], while Rippe and Haraldsson considered the capillary surface area [16, 41] as a suitable measure. Looking at the fractional lymph flow rate values in detail, the one for the lung is among the lowest, but this needs to be seen in the context of this organ conveying the entire cardiac plasma output. Likewise, two-pore mediated extravasation of proteins is not necessarily the only process affecting organ interstitial concentrations either. In the case of brain, whilst the low value for J_{br} is in line with the very limited permeability of the blood–brain barrier, the interstitial protein concentrations are further reduced by the rapid removal of any modalities which do cross the blood–brain barrier through extravasation or transcytosis by the CSF flow which receives fluid via aquaporins and excludes proteins altogether [58, 59]. Although most of the tissue lymph flow values are similar between the for the *SB* and *BM* physiological parameter sets, there are also significant difference, most notably for the heart, where the gap is 30-fold. Interestingly, Eigenmann et al. [44] and Niederalt estimates [13] fall between the two but the overall conclusion is that physiological parameter values may significantly affect the least squares PBPK fitting results and it is highly desirable to evaluate and adopt a standard set to facilitate the comparison of modelling efforts from different labs.

Niederalt et al. [13] chose to establish the correlation between J_{org} and $J_{iso,org}$ parameters by curve-fitting. Notably, the correlation factor $f_{Jiso,org}$ had values ranging from 0.01 to 0.96 (mean 0.5 ± 0.4), which are in good agreement with the prediction from our two-pore model which predicts the typical value of 0.45 (range 0.3–0.7). This suggests similar underlying performance for the two models based on the shared underlying framework, while more detailed physiology in the form of venous plasma

Table 5 Endosomal parameters in mice and rats based on PBPK model variant 1.SB

Parameters (units)	Description	Mice		Rat	
		Albumin	IgG	Albumin	IgG
Parameters					
k_{up} (1/h)	Rate constant for endosomal uptake	0.9	0.9	0.9	0.9
k_{rec} (1/h)	Rate constant for endosomal recycling	23.37	11.7	23.37	11.7
MRT (min)	Mean residence time	2.5	5	2.5	5
k_{deg} (1/h)	Rate constant for endosomal degradation	152.8	152.8	152.8	152.8
k_{rec}/k_{deg}	Recycling/degradation ratio	1	12.5	1	60
PBPK predictions					
$[X]_{endosome}/[X]_{plasma}$	Free endosomal to plasma concentration ratio	0.0025	0.0015	0.013	0.0007
$[X]_{lymph}/[X]_{plasma}$	Free Lymph to plasma concentration ratio	0.55	0.5	0.53	0.5
FcRn occupancy (%)	Bound FcRn fraction/total FcRn	37	19	60	38

PBPK predictions based on *1.SB* model variant

X represents a protein modality

pool and distinct segments of gastrointestinal tract was used by Niederalt, as well as estimates for organ-specific PS_{org} values derived from independently available experimental data.

Derivation of other PBPK model outcomes

The PBPK model allows derivation of the respective contribution of filtration (J_{org} and $J_{org,ISO}$) and diffusion (PS_{org}) to the extravasation of soluble proteins through large and small pores for all organs using the Peclet number values for large and small pores (Pe_L and Pe_S) as described in our previous work [6]. The values of Pe_L and Pe_S derived from the PBPK variant models, together with the glomerular filtration coefficient (Θ) calculated from the Stokes radius of the proteins, are listed in Supplementary Table 5 for the different modalities. The size of the protein significantly affects the rate of renal elimination: for larger proteins, like albumin and IgG, this elimination route is negligible, whereas it is significant for the smaller ones like dAb2 (DMS5558) which is estimated to be 95% renally excreted [12]. About 5% of cardiac plasma output passes through the glomerular barrier and it takes about 4 min in mice for the entire plasma volume equivalent. This means that even very small amounts of AlbudAb^{TM} free fraction can rapidly be removed from circulation. Rapid central elimination, in turn, results in a situation where, by the end of the relatively short distribution phase, the plasma concentration of dAb2 will have decreased below that in the organ interstitial spaces so that the net flux across the vascular barrier changes its direction due to the reversed concentration gradient. As a result, unlike for albumin and IgG, no pseudo steady-state tissue distribution flux value is achieved for the 23.6 kDa dAb2 molecule following a single bolus IV dose (see Supplementary Fig. 7A). As the size of the protein increases, as simulated for Fab and Fab2 in Supplementary Fig. 7B and C, this flux reversal phenomenon becomes less dominant and is not expected at all to take place for proteins with long half-lives like albumin and IgG (see Supplementary Fig. 7D, E). This can explain why the flux time course from Supplementary Fig. 7D, E mirrors the respective concentration–time course profiles in blood and organs from Fig. 3.

A number of mathematical models have been built to describe lymphatic circulation, describing processes such as lymph propulsion, flow-regulating valves in lymphatic vessels, pressure drop in secondary lymphoid organs and viscosity [20]. As the picture remains fragmented, these processes were not incorporated in our model. Moreover, large molecule PBPK models, except the one by Heiskanen and Kairemo [60], postulate unidirectional fluid flow from vascular capillaries into interstitial space, as pointed out by Jones et al. [61] while the classic Starling principle maintains that a relatively large (but unspecified) fraction of capillary plasma enters the interstitial space from the arterial side of capillaries, exits from the venous side and leaves behind a trickle to form the lymph flow [48]. The isogravimetric flow in the two-pore models may account to some extent for that local circulation but the situation can be more complex. According to Levick and Michel [62], when the Starling hypothesis is modified to consider the plasma protein gradients at the glycocalyx-filled paracellular pores, there is no need for the capillary venous side reflux to take place at all. This implies though that the interstitial compartment should not be considered as well-

mixed, which is incompatible with the current approaches to PBPK.

We fitted the endosomal recycling part of the model very frugally, with just the recycling rate constant for albumin ($k_{rec,albumin}$) estimated empirically. FcRn endosomal concentrations values were fixed to literature values, the non-specific rate constant for uptake (k_{up}) was derived from NCA results, and the recycling rate for IgG ($k_{rec,IgG}$) together with the degradation rate for all endosomal modalities not bound to FcRn (k_{deg}) were derived from the PBPK model estimates. All those parameters are listed in Table 5 for the model variant *1.SB*. The mean residence time for FcRn complexes in the endosomal compartment were obtained from their respective recycling rate value ($MRT = 1/k_{rec}$) and were approximately at 2.5 min for albumin and 5 min for IgG1. This is in line with the earlier estimates [27, 63–65], including direct measurements by Tzaban et al. [66]. While the recycling/degradation ratio for albumin at steady-state was constrained to 1 by Eq. 5, the equivalent measure for IgG1 was 12.5 for mice and 60 for rats, higher than 4, the value estimated by Kim et al. [35] or 9 by Eigenmann et al. [67] in mice.

Two molecules of FcRn can bind IgG at the same time, which greatly complicates the affinity measurements by surface plasmon resonance with the immobilized receptor. Whilst resembling natural orientation, the dissociation process is avidity-dominated and reliable rate constant values can only be obtained if receptor cross-linking is avoided as shown by Abdiche et al. [40]. From the data presented in afore mentioned paper, we estimated the in vivo avidity coefficient of IgG for FcRn to be around 10, as described in the methods. This is less than the theoretical 10^4-fold limit for mAb binding to two cell surface targets [68] and may reflect steric hindrances as IgG interaction with FcRn may be more constrained than with membrane antigens. In contrast, FcRn interaction with albumin is monovalent and involves a binding site distinct from that used by IgG [28, 30]. The PBPK model predicted steady-state concentration of the endogenous albumin and IgG in the endosomal space as well as the FcRn occupancy are listed in Table 5.

The model-predicted endosomal steady-state concentrations of endogenous albumin and IgG are significantly lower than those in plasma, thereby reconciling the discrepancy between the in vitro measured affinity and in vivo estimated potency of IgG as analysed by Gurbaxani [69] and Xiao [70]. The results also indicate that in steady state conditions 37% of FcRn is bound by endogenous albumin in mice and 60% in rats, while for the endogenous IgG the respective values are 19 and 38%, with interspecies difference relating to the respective plasma concentration values and largely in line with estimates for human FcRn at 65% and 35% for albumin and IgG respectively by Kim et al. [71].

In addition to the endosomal characterisation of IgG and albumin, the PBPK model allows evaluating the plasma half-lives of AlbudAbs^{TM} as a function of their albumin-binding affinities. Whilst AlbudAbs^{TM} with higher affinity exhibited albumin-like plasma half-life, the ones with weaker affinity displayed gradually accelerating clearance, as confirmed by experimental data. The expected correlation between the AlbudAb^{TM} affinity for albumin and its terminal plasma half-life is shown on Fig. 7, where good to satisfactory match with the experimental data is observed. Surprisingly, relatively high affinity of Kd < 100 nM is required for AlbudAbs^{TM} to reach and to maintain albumin-like half-life despite a high concentration of albumin in mouse plasma ($\sim$ 340 μM). This relationship derived from PBPK model predictions could be used as a quantitative tool to select the right AlbudAb^{TM} modality as it allows the estimation of the Kd (even not tested experimentally) for a specified plasma half-life.

Limitation of the PBPK model

Even the most complex PBPK models do not capture all the physiological complexity. They are also shaped and limited by the current state of scientific knowledge where considerable gaps and diversity of opinions still exist. Like with our earlier approach [12], the current model too is based on many assumptions: all compartments are well-stirred, the hydrostatic and oncotic pressure differences across the endothelial barrier are the same in all organs and macropinocytosis is limited to the FcRn-expressing cells only, while the receptor itself is confined to the endosomal compartment only. Likewise, the Patlak equation, which underpins the two-pore transport in this and other models based on it, describes a steady-state system where infinitely diluted spherical uncharged particles diffuse and filter through perfectly cylindrical channels. We appreciate that protein disposition may be affected by factors beyond the molecular weight such as, shape, charge or hydrophobicity, which were not considered in our current work, while the paracellular channels are thought to be tortuously irregular and crowded with other plasma proteins, all of which requires further analysis and implementation, if desirable.

Conclusions

Despite the limitations, we expect the model described in this work, as well as those described by other groups, to facilitate the adoption of PBPK as a standard tool for human dose prediction for biologics in the spirit of the Three Pillars Paradigm [72] by providing mechanistic

framework to analyse tissue penetration, turnover and target engagement of biologic drugs [73]. The model building tools described and developed should allow to build more comprehensive system-based models that will link PK with PD in mechanistic fashion, as envisaged by Jones et al. [61].

Biological macromolecules can often engage a number different interaction partners and incorporation of these into the models can become so labour-intensive that manual coding becomes prohibitively time-consuming and error-prone. It is likely that without introducing computer-assisted model building, the first of a kind we are aware of, it would not have been feasible to assemble the model used in this work by hand even in the graphical desktop interface of SimBiology™.

Finally, to our knowledge this is the first PBPK model of albumin which can help to understand not only its own tissue distribution and turnover, but also that of many other endogenous and exogenous small proteins that bind to it, for example AlbudAbs™ for plasma half-life extension purposes.

Acknowledgements Milan Ovecka, Ed Coulstock, Leigh-Ann Booth, Laurent Jespers, Valeriu Damian-Iordache, Indranil Rao and Gaohua Lu, for generously sharing the data, supporting the study and revising the manuscript.

References

1. Carter PJ, Lazar GA (2017) Next generation antibody drugs: pursuit of the 'high-hanging fruit'. Nat Rev Drug Discov 17:197–223
2. Lagassé HAD, Alexaki A, Simhadri VL, Katagiri NH, Jankowski W, Sauna ZE, Kimchi-Sarfaty C (2017) Recent advances in (therapeutic protein) drug development. F1000Research 6:113
3. Ward ES, Gussow D, Griffiths AD, Jones PT, Winter G (1989) Binding activities of a repertoire of single immunoglobulin variable domains secreted from *Escherichia coli*. Nature 341(6242):544–546
4. Jespers L, Schon O, Famm K, Winter G (2004) Aggregation-resistant domain antibodies selected on phage by heat denaturation. Nat Biotechnol 22(9):1161–1165
5. Jespers L, Schon O, James LC, Veprintsev D, Winter G (2004) Crystal structure of HEL4, a soluble, refoldable human VH single domain with a germ-line Scaffold. J Mol Biol 337(4):893–903
6. Tijink BM, Laeremans T, Budde M, Walsum MS-V, Dreier T, de Haard HJ, Leemans CR, van Dongen GAMS (2008) Improved tumor targeting of anti-epidermal growth factor receptor nanobodies through albumin binding: taking advantage of modular nanobody technology. Mol Cancer Ther 7(8):2288–2297
7. Müller MR, Saunders K, Grace C, Jin M, Piche-Nicholas N, Steven J, O'Dwyer R, Wu L, Khetemenee L, Vugmeyster Y, Hickling TP, Tchistiakova L, Olland S, Gill D, Jensen A, Barelle CJ (2012) Improving the pharmacokinetic properties of biologics by fusion to an anti-HSA shark VNAR domain. mAbs 4(6):673–685
8. Holt LJ, Basran A, Jones K, Chorlton J, Jespers LS, Brewis ND, Tomlinson IM (2008) Anti-serum albumin domain antibodies for extending the half-lives of short lived drugs. Protein Eng Des Sel 21(5):283–288
9. Baxter LT, Zhu H, Mackensen DG, Jain RK (1994) Physiologically based pharmacokinetic model for specific and nonspecific monoclonal antibodies and fragments in normal tissues and human tumor xenografts in nude mice. Cancer Res 54(6):1517–1528
10. Ferl G, Wu A, DiStefano J (2005) A predictive model of therapeutic monoclonal antibody dynamics and regulation by the neonatal Fc receptor (FcRn). Ann Biomed Eng 33(11):1640–1652
11. Gill K, Gardner I, Li L, Jamei M (2015) A bottom-up whole-body physiologically based pharmacokinetic model to mechanistically predict tissue distribution and the rate of subcutaneous absorption of therapeutic proteins. AAPS J. https://doi.org/10.1208/s12248-015-9819-4
12. Sepp A, Berges A, Sanderson A, Meno-Tetang G (2015) Development of a physiologically based pharmacokinetic model for a domain antibody in mice using the two-pore theory. J Pharmacokinet Pharmacodyn 42(2):97–109
13. Niederalt C, Kuepfer L, Solodenko J, Eissing T, Siegmund H-U, Block M, Willmann S, Lippert J (2018) A generic whole body physiologically based pharmacokinetic model for therapeutic proteins in PK-Sim. J Pharmacokinet Pharmacodyn 45(2):235–257
14. Garg A, Balthasar J (2007) Physiologically-based pharmacokinetic (PBPK) model to predict IgG tissue kinetics in wild-type and FcRn-knockout mice. J Pharmacokinet Pharmacodyn 34(5):687–709
15. Hansen RJ, Balthasar JP (2003) Pharmacokinetic/pharmacodynamic modeling of the effects of intravenous immunoglobulin on the disposition of antiplatelet antibodies in a rat model of immune thrombocytopenia. J Pharm Sci 92(6):1206–1215
16. Rippe B, Haraldsson B (1994) Transport of macromolecules across microvascular walls: the two-pore theory. Physiol Rev 74(1):163–219
17. Shah DK, Betts AM (2012) Towards a platform PBPK model to characterize the plasma and tissue disposition of monoclonal antibodies in preclinical species and human. J Pharmacokinet Pharmacodyn 39(1):67–86
18. Meno-Tetang GML, Li H, Mis S, Pyszczynski N, Heining P, Lowe P, Jusko WJ (2006) Physiologically based pharmacokinetic modeling of FTY720 (2-amino-2[2-(-4-octylphenyl)ethyl]propane-1,3-diol hydrochloride) in rats after oral and intravenous doses. Drug Metab Dispos 34(9):1480–1487
19. Kelch ID, Bogle G, Sands GB, Phillips ARJ, LeGrice IJ, Rod Dunbar P (2015) Organ-wide 3D-imaging and topological analysis of the continuous microvascular network in a murine lymph node. Sci Rep 5:16534
20. Margaris KN, Black RA (2012) Modelling the lymphatic system: challenges and opportunities. J R Soc Interface 9:601–612
21. Graf JF, Scholz BJ, Zavodszky MI (2012) BioDMET: a physiologically based pharmacokinetic simulation tool for assessing proposed solutions to complex biological problems. J Pharmacokinet Pharmacodyn 39(1):37–54
22. Boswell CA, Mundo EE, Ulufatu S, Bumbaca D, Cahaya HS, Majidy N, Van Hoy M, Schweiger MG, Fielder PJ, Prabhu S, Khawli LA (2014) Comparative physiology of mice and rats: radiometric measurement of vascular parameters in rodent tissues. Mol Pharm 11(5):1591–1598
23. Wiig H, Gyenge C, Iversen PO, Gullberg D, Tenstad O (2008) The role of the extracellular matrix in tissue distribution of macromolecules in normal and pathological tissues: potential therapeutic consequences. Microcirculation 15(4):283–296
24. Bos NA, Kimura H, Meeuwsen CG, Visser HD, Hazenberg MP, Wostmann BS, Pleasants JR, Benner R, Marcus DM (1989) Serum immunoglobulin levels and naturally occurring antibodies

against carbohydrate antigens in germ-free BALB/c mice fed chemically defined ultrafiltered diet. Eur J Immunol 19(12):2335–2339
25. Fan Y-Y, Avery LB, Wang M, O'Hara DM, Leung S, Neubert H (2016) Tissue expression profile of human neonatal Fc receptor (FcRn) in Tg32 transgenic mice. mAbs 8(5):848–853
26. D'Hooghe L, Chalmers AD, Heywood S, Whitley P (2017) Cell surface dynamics and cellular distribution of endogenous FcRn. PLoS ONE 12(8):e0182695
27. Chen Y, Balthasar JP (2012) Evaluation of a catenary PBPK model for predicting the in vivo disposition of mAbs engineered for high-affinity binding to FcRn. AAPS J 14(4):850–859
28. Chaudhury C, Brooks CL, Carter DC, Robinson JM, Anderson CL (2006) Albumin binding to FcRn: distinct from the FcRn–IgG interaction. Biochemistry 45(15):4983–4990
29. Cameron J, Sleep D, Sandlie I, Andersen JT (2014) Pharmacokinetic animal model. Google Patents
30. Chaudhury C, Mehnaz S, Robinson JM, Hayton WL, Pearl DK, Roopenian DC, Anderson CL (2003) The major histocompatibility complex-related Fc receptor for IgG (FcRn) binds albumin and prolongs its lifespan. J Exp Med 197(3):315–322
31. Junghans RP, Anderson CL (1996) The protection receptor for IgG catabolism is the beta2-microglobulin-containing neonatal intestinal transport receptor. Proc Natl Acad Sci USA 93(11):5512–5516
32. Ghetie V, Hubbard JG, Kim J-K, Tsen M-F, Lee Y, Ward ES (1996) Abnormally short serum half-lives of IgG in β2-microglobulin-deficient mice. Eur J Immunol 26(3):690–696
33. Bazin-Redureau MI, Renard CB, Scherrmann J-MG (1997) Pharmacokinetics of heterologous and homologous immunoglobulin G, F(ab')2 and Fab after intravenous administration in the rat. J Pharm Pharmacol 49(3):277–281
34. Nolte H, Hölper S, Selbach M, Braun T, Krüger M (2014) Assessment of serum protein dynamics by native SILAC flooding (SILflood). Anal Chem 86(22):11033–11037
35. Kim J, Bronson CL, Hayton WL, Radmacher MD, Roopenian DC, Robinson JM, Anderson CL (2006) Albumin turnover: FcRn-mediated recycling saves as much albumin from degradation as the liver produces. Am J Physiol—Gastrointest Liver Physiol 290(2):G352–G360
36. Anderson CL, Chaudhury C, Kim J, Bronson CL, Wani MA, Mohanty S (2006) Perspective—FcRn transports albumin: relevance to immunology and medicine. Trends Immunol 27(7):343–348
37. Zaias J, Mineau M, Cray C, Yoon D, Altman NH (2009) Reference values for serum proteins of common laboratory rodent strains. J Am Assoc Lab Anim Sci: JAALAS 48(4):387–390
38. Hay JB, Hobbs BB (1977) The flow of blood to lymph nodes and its relation to lymphocyte traffic and the immune response. J Exp Med 145(1):31–44
39. Herman PG, Lyonnet D, Fingerhut R, Tuttle RN (1976) Regional blood flow to the lymph node during the immune response. Lymphology 9(3):101–104
40. Abdiche YN, Yeung YA, Chaparro-Riggers J, Barman I, Strop P, Chin SM, Pham A, Bolton G, McDonough D, Lindquist K, Pons J, Rajpal A (2015) The neonatal Fc receptor (FcRn) binds independently to both sites of the IgG homodimer with identical affinity. mAbs 7(2):331–343
41. Rippe B, Haraldsson B (1987) On the steady-state relationship between the microvascular hydrostatic pressure and the transvascular filtration rate. Effects of heteroporosity. Acta Physiol Scand 129(3):441–442
42. Granger DN, Miller T, Allen R, Parker RE, Parker IC, Taylor AE (1979) Permselectivity of cat liver blood-lymph barrier to endogenous macromolecules. Gastroenterology 77(1):103–109
43. Akaike H (1976) An information criterion (AIC). Math Sci 14(153):5–9
44. Eigenmann MJ, Karlsen TV, Krippendorff B-F, Tenstad O, Fronton L, Otteneder MB, Wiig H (2017) Interstitial IgG antibody pharmacokinetics assessed by combined in vivo- and physiologically-based pharmacokinetic modelling approaches. J Physiol 595(24):7311–7330
45. Covell DG, Barbet J, Holton OD, Black CD, Parker RJ, Weinstein JN (1986) Pharmacokinetics of monoclonal immunoglobulin G1, F(ab')2, and Fab' in mice. Cancer Res 46(8):3969–3978
46. Rao IR, Rose R, Li L (2016) Predicting pharmacokinetics and pharmacodynamics of therapeutic proteins. In: Biologics Focussed Workshop, Sheffield, Simcyp
47. Levick JR (1987) Flow through interstitium and other fibrous matrices. Exp Physiol 72(4):409–437
48. Caro CG, Pedley TJ, Schroter RC, Seed WA (2011) The mechanics of the circulation, 2nd edn. Cambridge University Press, Cambridge
49. Brambell FW, Hemmings WA, Morris IG (1964) A theoretical model of gamma-globulin catabolism. Nature 203:1352–1354
50. Scott CC, Vacca F, Gruenberg J (2014) Endosome maturation, transport and functions. Semin Cell Dev Biol 31:2–10
51. French AR, Lauffenburger DA (1997) Controlling receptor/ligand trafficking: effects of cellular and molecular properties on endosomal sorting. Ann Biomed Eng 25(4):690–707
52. Sari L, Bjoern J, Michael BO, Annika H, Sven K (2017) Distribution of FcRn across species and tissues. J Histochem Cytochem 65(6):321–333
53. Fan Y-Y, Neubert H (2016) Quantitative analysis of human neonatal Fc receptor (FcRn) tissue expression in transgenic mice by online peptide immuno-affinity LC-HRMS. Anal Chem 88(8):4239–4247
54. Wiśniewski JR, Ostasiewicz P, Duś K, Zielińska DF, Gnad F, Mann M (2012) Extensive quantitative remodeling of the proteome between normal colon tissue and adenocarcinoma. Mol Syst Biol 8(1):611
55. Gaizutis M, Pesce AJ, Pollak VE (1975) Renal clearance of human and rat albumins in the rat. Proc Soc Exp Biol Med 148(4):947–952
56. Sarin H (2010) Physiologic upper limits of pore size of different blood capillary types and another perspective on the dual pore theory of microvascular permeability. J Angiogenesis Res 2(1):1–19
57. Dostalek M, Gardner I, Gurbaxani BM, Rose RH, Chetty M (2013) Pharmacokinetics, pharmacodynamics and physiologically-based pharmacokinetic modelling of monoclonal antibodies. Clin Pharmacokinet. https://doi.org/10.1007/s40262-012-0027-4
58. Johanson CE, Duncan JA, Klinge PM, Brinker T, Stopa EG, Silverberg GD (2008) Multiplicity of cerebrospinal fluid functions: new challenges in health and disease. Cerebrospinal Fluid Res 5:10–10
59. Brinker T, Stopa E, Morrison J, Klinge P (2014) A new look at cerebrospinal fluid circulation. Fluids Barriers CNS 11:10–10
60. Heiskanen T, Kairemo K (2009) Development of a PBPK model for monoclonal antibodies and simulation of human and mice PBPK of a radiolabelled monoclonal antibody. Curr Pharm Des 15(9):988–1007
61. Jones HM, Mayawala K, Poulin P (2013) Dose selection based on physiologically based pharmacokinetic (PBPK) approaches. AAPS J 15:377–387
62. Levick JR, Michel CC (2010) Microvascular fluid exchange and the revised Starling principle. Cardiovasc Res 87(2):198–210
63. Gurbaxani B, Dostalek M, Gardner I (2013) Are endosomal trafficking parameters better targets for improving mAb

pharmacokinetics than FcRn binding affinity? Mol Immunol 56(4):660–674
64. Schröter C, Günther R, Rhiel L, Becker S, Toleikis L, Doerner A, Becker J, Schönemann A, Nasu D, Neuteboom B, Kolmar H, Hock B (2015) A generic approach to engineer antibody pH-switches using combinatorial histidine scanning libraries and yeast display. mAbs 7(1):138–151
65. Hopkins CR, Trowbridge IS (1983) Internalization and processing of transferrin and the transferrin receptor in human carcinoma A431 cells. J Cell Biol 97(2):508–521
66. Tzaban S, Massol RH, Yen E, Hamman W, Frank SR, Lapierre LA, Hansen SH, Goldenring JR, Blumberg RS, Lencer WI (2009) The recycling and transcytotic pathways for IgG transport by FcRn are distinct and display an inherent polarity. J Cell Biol 185(4):673–684
67. Eigenmann MJ, Fronton L, Grimm HP, Otteneder MB, Krippendorff B-F (2017) Quantification of IgG monoclonal antibody clearance in tissues. mAbs 9(6):1007–1015
68. Sengers BG, McGinty S, Nouri FZ, Argungu M, Hawkins E, Hadji A, Weber A, Taylor A, Sepp A (2016) Modeling bispecific monoclonal antibody interaction with two cell membrane targets indicates the importance of surface diffusion. mAbs 8(5):905–915
69. Gurbaxani B (2007) Mathematical modeling as accounting: predicting the fate of serum proteins and therapeutic monoclonal antibodies. Clin Immunol 122(2):121–124
70. Xiao JJ (2012) Pharmacokinetic models for FcRn-mediated IgG disposition. J Biomed Biotechnol 2012:282989
71. Kim J, Hayton WL, Robinson JM, Anderson CL (2007) Kinetics of FcRn-mediated recycling of IgG and albumin in human: pathophysiology and therapeutic implications using a simplified mechanism-based model. Clin Immunol 122(2):146–155
72. Morgan P, Van Der Graaf PH, Arrowsmith J, Feltner DE, Drummond KS, Wegner CD, Street SDA (2012) Can the flow of medicines be improved? Fundamental pharmacokinetic and pharmacological principles toward improving Phase II survival. Drug Discov Today 17(9–10):419–424
73. Phair RD (2014) Mechanistic modeling confronts the complexity of molecular cell biology. Mol Biol Cell 25(22):3494–3496